NUMERICAL AND EXPERIMENTAL INVESTIGATION OF THE TEMPERATURE DISTRIBUTION INSIDE OIL-COOLED TRANSFORMER WINDINGS

N. Schmidt[1*] and S. Tenbohlen[1] and S. Chen[2] and C. Breuer[3]

[1]University of Stuttgart, Pfaffenwaldring 47, 70569 Stuttgart, Germany
[2]ALSTOM Grid, 129 Avenue de Paris 91300 Massy, France
[3]ALSTOM Grid, Rheinstrasse 73, 41065 Mönchengladbach, Germany
*Email: nicolas.schmidt@ieh.uni-stuttgart.de

Abstract: This contribution describes the thermal investigation of an oil-cooled transformer winding by means of an experimental and a two-dimensional numerical winding model. At first, the two created models are described in detail, pointing out all assumptions and simplifications applied during the respective modelling process. Subsequently, an appropriate discretization scheme of the numerical model for computational fluid dynamics (CFD) simulations is determined. Since the two models resemble a common winding design, a validation of the numerical results with the experimental data is carried out. It shows an acceptable agreement of the respective results depending on the chosen boundary conditions. In addition, short comings of the two dimensional approach pursued for the numerical model are identified and discussed.

1 INTRODUCTION

The power rating and lifetime of power transformers is strongly dependent on the chosen thermal design. The higher the temperatures at a given loading rate are settling, the faster the paper insulation of a transformer will degenerate. A temperature increase of approximately 6 to 8 K doubles the depolymerisation rate of cellulose [1]. The highest temperature developing within the insulation therefore determines the aging rate of the entire component. For that reason, detailed knowledge about the temperature distribution inside transformer windings is necessary to assess a proper power rating resulting in a desired minimum service lifetime. A thoroughly thermal investigation via direct measurements in power transformers poses several challenges being difficult to be met. Beside the determination of prevailing boundary conditions, the accuracy and proper placement of measurement equipment suitable for an application inside a transformer in operation are notable examples in addition to monetary aspects. Consequently, winding models are applied for the thermal analysis of power transformers.

2 INVESTIGATED WINDING MODELS

The modelling approach pursued within this investigation applies certain simplifications to keep the associated efforts and expenses for the respective models in reasonable boundaries. To illustrate some of those simplifications, Figure 1 shows a three phase core type power transformer in very low detail. The first assumption for creating the numerical and experimental winding models is that any heat transfer in radial direction is neglected. This comprises the heat applied by the core to the windings, heat transfer between the LV- and HV-windings and heat transferred to the cooling oil outside of the windings.

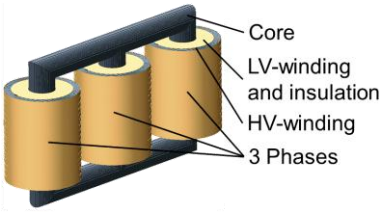

Figure 1: Simplified model of a three phase core type power transformer

To picture the additional modelling steps, Figure 2 shows a section of a disc type HV-winding with six conductors in radial direction. For reasons of improved visibility, the outer cardboard cylinder is displayed transparent.

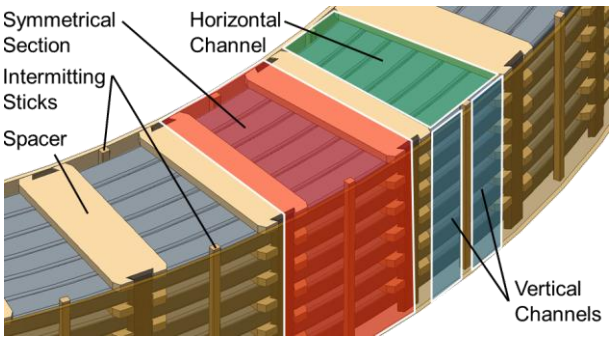

Figure 2: Example for a section of an HV-winding in a three dimensional perspective

The applied spacers create a defined distance between two discs in axial direction. Combined with their axial fixations they divide each winding in circumferential direction into symmetrical sections forming horizontal and vertical oil channels. Taking advantage of that symmetry, the created winding models resemble just one of those symmetrical sections. However, it should be noted that this approach assumes symmetrical boundary conditions in circumferential direction of the investigated winding. Unlike the HV-winding design shown in Figure 2 with 6 conductors in one disc, the investigated winding models correlate to an LV-winding with only one conductor in radial direction. In addition, spacers are only placed every second disc in axial direction, leaving pairs of conductors separated by spacers. The cross section shown in Figure 3 displays the layout of the winding model analysed within this investigation. It resembles three passes of an LV-winding designed with representative dimensions. The winding's centre would be on the left side of the cross section shown in Figure 3, resulting in widening horizontal channels in the second and narrowing horizontal channels in the third pass.

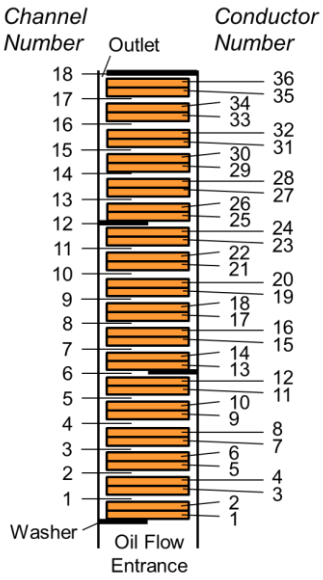

Figure 3: Layout of the experimental winding model including reference to conductor and channel number

2.1 Experimental Winding Model

Figure 4 shows an experimental conductor model used within this investigation. The raw material copper is partially displayed transparent to improve visibility. Heating cartridges were put inside drilled holes within these conductor models to impress the power that would results from electrical losses in actual conductors. In addition, Pt100 sensors were put into a second drill hole inside each conductor model. The top and bottom surface of the conductor models were machined with a texture resembling the surface of CTC-Conductors.

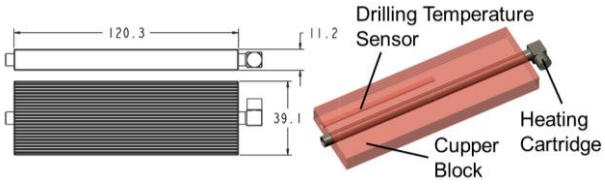

Figure 4: Experimental conductor model with heating cartridge (dimensions in [mm])

The spacers used for the experimental winding model are designed to cover an area correlating to the length of the conductor models representing one section in circumferential direction. It can be noted that the bending of the actual conductors in circumferential direction is neglected for the conductor models. Nevertheless, resulting from the spacer's placement shown in Figure 5, the variable width of the resulting horizontal channels correlates with the width in an actual winding. The front and back surfaces applied with drilling holes were insulated with foam sealing to minimize any heat transfer in circumferential direction inexistent in an actual winding. The inner and outer cardboard cylinders were replaced by sheets of acrylic glass.

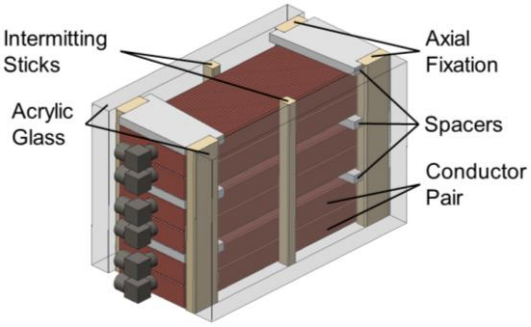

Figure 5: Arrangement of the conductor models to from a part of the LV-winding design

The experimental setup used for this investigation comprises components to create constant and defined boundary conditions. To control the oil flow rate a pump fed oil through a controlled flap operated with sensor information of a flow meter. Defined oil temperatures at the inlet of the winding model were realized with a controlled flow heater. Detailed information about the experimental setup and procedure can be found in [2]. In addition to the losses applied in the heat cartridges, the oil flow rate and the inlet temperature of oil entering the winding model were set to varied values given in Table 1. It should be noted that the given values concerning the oil flow rate correspond to the oil flow entering an entire LV-winding with corresponding characteristics and not just one symmetrical section. Also the losses per conductor refer to the losses in one complete winding turn and not to the conductor part in one symmetrical section.

Table 1: Set of boundary conditions applied for the experimental investigation with all values referring to one LV-winding

Boundary Condition					
Oil flow rate $\dot{m}_{oil}$ [kg/s]	2.1	3.5	7.0	10.5	12.6
Inlet temperature ϑ_{in} [°C]	35	50	70	90	
Losses per conductor P_{loss} [W]	630	1050			

2.2 Numerical Winding Model

The numerical winding model was created using the commercial software ANSYS ICEM CFD and ANSYS CFX. Since the thoroughly representation of the third dimension orthogonal to the main oil flow requires extensive computational efforts, the numerical winding model applied for analysis within this contribution is 2-dimensional (2-D). However, ANSYS CFX does not employ a separate 2-D solver. For that reason, 2-D meshes have to be extruded into the third dimension creating one layer of three-dimensional cells. Since the thickness of this layer can be formulated variably, this offers the benefit that the numerical winding model can take the widening and narrowing of all channels in radial direction into account. Nevertheless, the restriction of the oil flow at the side faces of the spacers is neglected. Since the spacers are covering a certain area of the heat transferring surface on the conductors, the numerical model assumes no heat transfer at those areas. Consequently the applied losses are concentrated into the parts of the conductors not covered by spacers. Additionally, the displayed intermitting sticks shown in Figure 5 restrict the oil flow and the connected heat transfer to some extent. Accordingly, two different treatments for these assembly elements have been implemented. In a first scenario, they are neglected entirely, resulting in decreased oil flow velocities in the vertical channels and in a simplified oil flow inside the horizontal channels. In the second scenario, they are treated as complete blockings in the vertical and horizontal channels also resulting in a simplified oil flow in the horizontal channels. Additionally, this approach decreases the surface available for cooling and increases the oil flow velocities in the horizontal channels. A comparison of the described treatments is part of this investigation and will be referred to as "*without sticks*" for the first scenario and "*with sticks*" for the second scenario.

3 MESH SENSITIVITY ANALYSIS

Prior to the numerical analysis of the investigated transformer winding the respective model has to be discretized. Since the gathered results ought to be independent of the chosen mesh density, a mesh sensitivity analysis was brought out. Figure 6 shows a conductor pair including the surrounding oil channels. Characteristic dimensions of interest for discretization are marked and enlargements of the three created meshes are displayed. Table 2 gives further detail regarding these characteristic dimensions and their discretization in Mesh 1, 2 and 3.

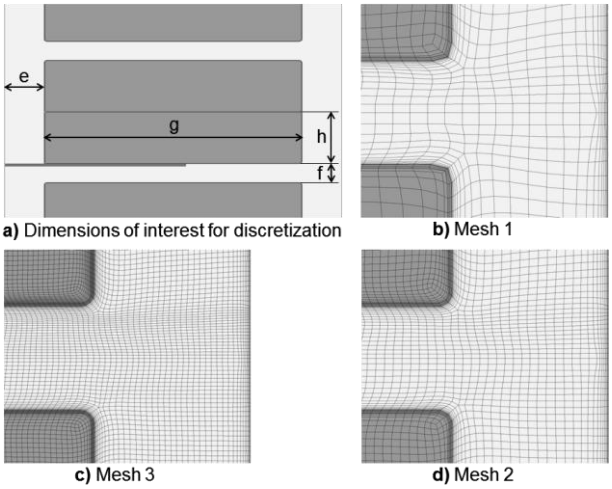

Figure 6: Marked dimensions of interest for discretization and enlargement of the investigated meshes with clockwise increasing mesh density

Table 2: Details about the chosen mesh densities for the dimensions of interest

	e	f	g	h
Physical dimension [mm]	6.0	4.0	39.2	11.2
Nodes in Mesh 1	28	28	60	20
Nodes in Mesh 2	36	36	120	40
Nodes in Mesh 3	44	44	180	60

Two representative operating states were chosen to compare the results in the different discretization schemes. In both states, the oil flow rate was set to $\dot{m}_{oil}$ = 10.5 kg/s and the losses per conductor were set to P_{loss} = 630 W. However, the inlet temperature for the first operating state was set to ϑ_{in} = 35 °C, resulting in a dynamic viscosity of $\eta_{oil} = 8.1 \cdot 10^{-3}$ Pa·s at the respective density of $\rho_{oil} = 864.25$ kg/m^3. For the second state the inlet temperature was set to ϑ_{in} = 70 °C, resulting in a dynamic viscosity of $\eta_{oil} = 3.0 \cdot 10^{-3}$ Pa·s at the respective density of $\rho_{oil} = 841.5$ kg/m^3. For engineering purposes, many characteristics concerning the flow and heat transfer are described applying the Reynolds number *Re* of the respective flow. This number can be calculated by

$$Re = \rho \cdot v \cdot d_h / \eta \qquad (1)$$

with the flow velocity v and the hydraulic diameter d_h. Estimating a hydraulic diameter of d_h = 0.01 m and a velocity of v = 1 m/s results in a Reynolds number of Re = 1067 for the first operating state

and Re = 2804 for the second operating state. While a laminar simulation setup was sufficient for the first operating state, a turbulent setup became necessary to achieve converging solutions at the second operating state. The applied turbulence model is the Shear Stress Transport model (SST) with the activated transitional turbulence Gamma Theta model and the Langtry Menter transition onset correlation. Since turbulence models are sensitive to the thickness of the first layer of cells within the boundary layer, this value is kept at 0.01 mm for all meshes. The first operating state will be referred to as "*laminar*" while the second operating state will be referred to as "*turbulent*". With regard to the intermitting sticks, the chosen treatment for the mesh sensitivity analysis was set to "*without sticks*". Figure 7 shows the oil flow distribution inside the second and third pass of the winding model for the three discretization schemes. It can be noted that for both operating states the resulting oil flow distribution appears to be close to independent of the chosen mesh density.

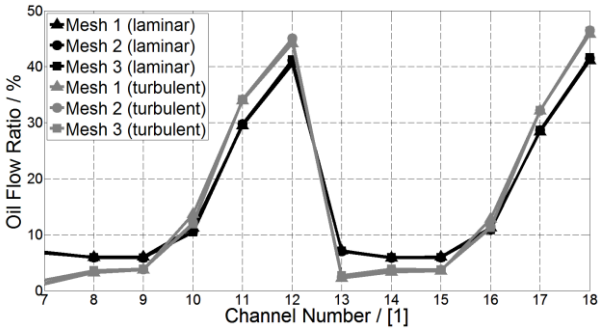

Figure 7: Comparison of the oil flow distribution inside the last two passes of the numerical winding model for the three different discretization schemes at laminar and turbulent conditions

Since the key interest of this investigation is the temperature distribution within transformer windings, Figure 8 shows the temperature gradients between each single conductor and the oil surrounding the respective conductor in the last two passes of the winding model. Therefore, the rise of the oil temperature within one pass was approximated by a linear function set between the inlet and outlet temperature within that pass. The boundary conditions were set to match the laminar operating state. It can be noted, that the deviations of the temperature gradients between Mesh 1 and Mesh 2 are on average at 0.4 K with a maximum of 0.8 K. In comparison, the deviations between Mesh 2 and Mesh 3 are significantly smaller, particularly with regard to the first conductor pair in each pass. On average, the resulting deviations between Mesh 2 and Mesh 3 are at 0.2 K with a maximum of 0.4 K. At the second operating state resulting in turbulent conditions, the deviations between the different discretization schemes given in Figure 9 are similar to the results at laminar conditions. While the deviations between Mesh 1 and Mesh 2 are on average at 0.5 K with a maximum of 1.1 K the results between Mesh 2 and Mesh 3 are almost identical. The average deviation is 0.1 K with a maximum of 0.2 K.

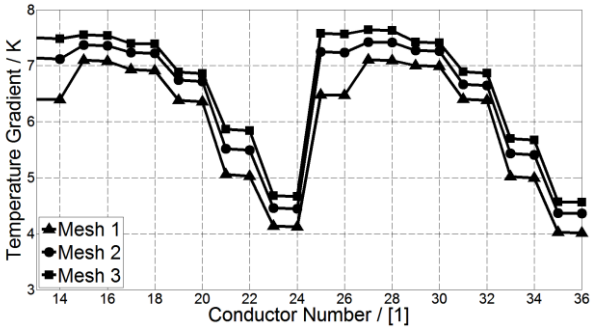

Figure 8: Comparison of the temperature gradients between oil and conductors inside the last two passes of the numerical winding model for three different discretization schemes at laminar conditions

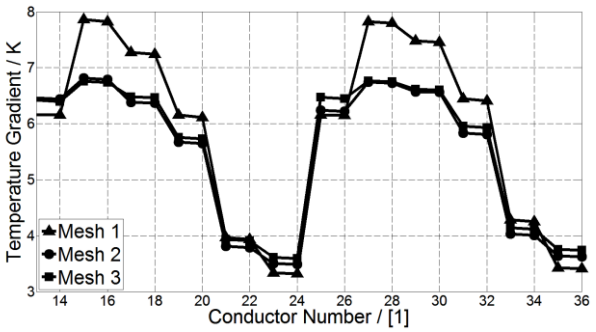

Figure 9: Comparison of the temperature gradients between oil and conductors inside the last two passes of the numerical winding model for three different discretization schemes at turbulent conditions

Summing up the results from the mesh sensitivity analysis, the discretization scheme Mesh 2 already yields reliable results with regard to numerical accuracy at the investigated operating states. Due to the minor deviations concerning the temperature distribution at laminar conditions between Mesh 2 and Mesh 3, the chosen discretization scheme for the numerical analysis presented in this contribution is Mesh 3. It should be borne in mind that the discretization parameters for Mesh 3 given in Table 2 might not be sufficient for all winding designs. They rather should be taken as a suggestion for future investigations and be validated when a high numerical accuracy is required.

4 COMPARISON BETWEEN EXPERIMENTAL AND NUMERICAL RESULTS

Since the developed winding models correlate to the same winding, a validation of the numerical

results by experimental data can be carried out. The Figures 10 to 13 give the temperature gradients between oil and conductors in the last two passes of the winding models at various conditions. The results derived from the numerical investigations are marked by circles in case of the modelling scenario neglecting the intermitting sticks entirely, as described in section 2.2. Results obtained with the modelling scenario perceiving the sticks as complete blockings are marked by triangles. The measurements conducted with the experimental winding model are marked by squares. For the determination of the oil temperature at a certain conductor, a linear approximation between the measured or calculated inlet and outlet temperature was applied.

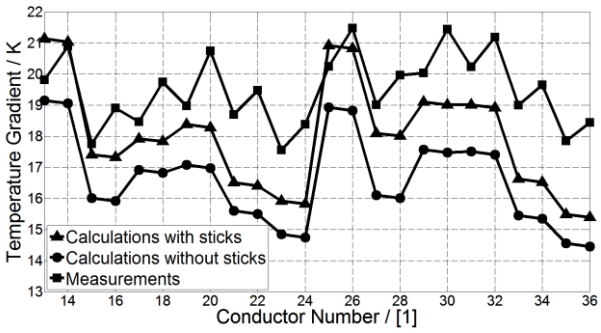

Figure 10: Comparison of the temperature gradients between oil and conductors inside the last two passes of the experimental and numerical winding model in laminar setup at ϑ_{in} = 35 °C, $\dot{m}_{oil}$ = 3.5 kg/s and P_{loss} = 1050 W

Figure 10 shows the experimental and numerical results at a low oil flow rate and inlet temperature. The simulation setup was set laminar. Regarding the two different numerical modelling scenarios, the temperature gradients in the scenario with stick are across both passes approximately 5-10 % higher compared to the scenario without sticks. Since the measured temperature gradients are another 5-10 % higher compared to the scenario with sticks, this scenario is closer to the measurements. Concerning the thermal coupling between each two conductors forming a conductor pair, the measurements give significant differences in temperature gradients of up to 10 % not matched by the numerical results. Aside from this, the temperature distribution is predicted similarly by all models. At the given boundary conditions, a high temperature gradient at the first conductor pair is followed by lower gradients increasing till the middle of each pass. From the middle to the end of each pass, the gradients are decreasing again. The last conductor pair is cooled most efficiently. Increasing the oil flow rate changes the measured temperature gradients and the deviations between measurements and calculations significantly. In Figure 11 the temperature gradients given by the measurements maintain on an almost stable level through the first two thirds of each pass. Within the last third of each pass, the gradients are dropping about 20 %. The numerical models are in acceptable agreement with these results, but the drop of temperature gradients is predicted within the second half of each pass and is bigger in magnitude. Both modelling scenarios give temperature gradients about 20 % below the measurements at the last conductor pairs of each pass. The constant temperature gradients within the first half of each pass are approximately 10 % higher in the scenario with sticks compared to the scenario without sticks. Since the temperature gradient level in the first half of each pass predicted by the modelling scenario without sticks is in good agreement with the measurements, this scenario performs better in comparison to the scenario with sticks at the given boundary conditions.

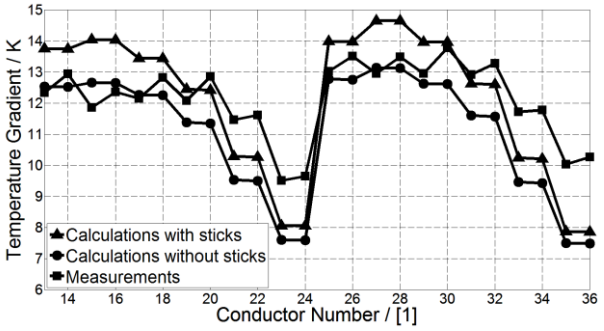

Figure 11: Comparison of the temperature gradients between oil and conductors inside the last two passes of the experimental and numerical winding model in laminar setup at ϑ_{in} = 35 °C, $\dot{m}_{oil}$ = 10.5 kg/s and P_{loss} = 1050 W

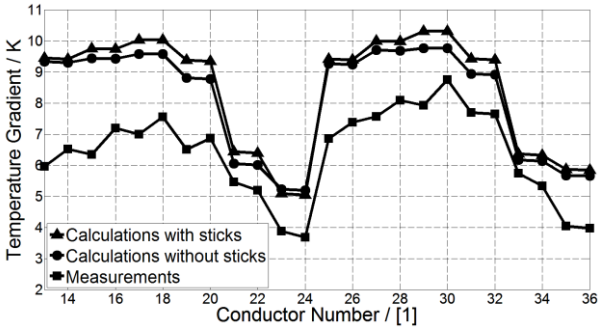

Figure 12: Comparison of the temperature gradients between oil and conductors inside the last two passes of the experimental and numerical winding model in turbulent setup at ϑ_{in} = 70 °C, $\dot{m}_{oil}$ = 12.6 kg/s and P_{loss} = 1050 W

As shown in Figure 12, the measured temperature gradients and the observable deviations between measurements and calculations change again considerably at high oil flow rates and high inlet temperatures. The measurements show a steady increase of temperature gradients within the first half of each pass followed by a twice as strong

decrease within the second half. This distribution is matched by both modelling scenarios with a slightly better performance of the scenario with sticks. However, there is a comparably constant offset around 25 % leading to an overestimation of the temperature gradients in both scenarios. Due to numerical reasons, a turbulence model as described in section 3 had to be applied to achieve converging numerical solutions at this operating state. Finally, Figure 13 displays the temperature gradients between conductors and oil at an operating state with a high inlet temperature but only a medium oil flow rate. Since by the application of a laminar setup a converging solution could still be obtained, the results of the laminar setup are given along the results of the turbulent setup. While the measured temperature gradients show a similar distribution compared to the operating state with a high inlet temperature and oil flow rate, the numerical results still resemble the results at low inlet temperatures and high oil flow rates. While the temperature gradients within the second half of each pass are in good agreement, substantial deviations between measurements and calculations regardless of the modelling scenario and calculation setup occur in the first half of each pass.

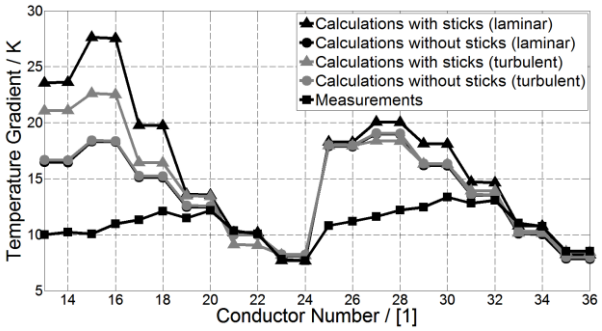

Figure 13: Comparison of the temperature gradients between oil and conductors inside the last two passes of the experimental and numerical winding model at ϑ_{in} = 70 °C, $\dot{m}_{oil}$ = 7.0 kg/s and P_{loss} = 1050 W

5 CONCLUSION

This contribution carried out a thermal investigation of a low voltage power transformer winding by means of an experimental and a numerical model. An appropriate mesh density for the numerical model was determined via a mesh sensitivity analysis. After describing both models in detail, the acquired experimental results were consulted for validation of the numerical model. Several conclusions can be drawn from this comparison. First of all, the thermal coupling of the experimental conductor pairs is probably weakened by the machined conductor surfaces. Since this is not taken into account within the numerical model, the thermal coupling is overestimated. Moreover, the observed agreement of measurements and calculations was found to be depended on the respective boundary conditions. At low inlet temperatures and oil flow rates, the displayed temperature distributions are in well agreement but show a 10 % offset regarding the temperature level. This results in an underestimation of the conductor temperatures with the numerical model. At high inlet temperatures and oil flow rates the agreement regarding the temperature distribution persists. However, a 25 % offset of the temperature level leads to an overestimation of the conductor temperatures with the numerical model. In between these boundary conditions, the agreement concerning the temperature distribution deteriorates. While at low temperatures and high oil flow rates the agreement is still acceptable, there are significant deviations at high inlet temperatures and moderate oil flow rates. A probable cause for this inconsistent agreement is a change of the respective flow characteristics, transitioning from a laminar to a turbulent behaviour. An accurate prediction of this complex phenomenon with a two dimensional model and a rather simple turbulence model is unlikely. For that reason, a three-dimensional winding model should be considered. In addition, the two-dimensional modelling approach is impeding the proper consideration of the intermitting sticks. The comparison of measurements and numerical results indicates a variant influence of the sticks also depending on the boundary conditions.

6 ACKNOWLEDGMENTS

This paper is published with the kind permission and support of ALSTOM Grid, Germany and France.

7 REFERENCES

[1] IEC 60076-7: Power Transformers Part 7: Loading guide for oil immersed power transformers, 2005

[2] N. Schmidt, A. Weinläder, S. Tenbohlen: „Experimental Investigation of the Temperature Distribution within the Low Voltage Winding of a Large Power Transformer“, ETG-Fachbericht 134, Diagnostik elektrischer Betriebsmittel 2012, Paper No. 54, ISBN 978-3-8007-3465-8